

Reasoning-Modulated Representations

Petar Veličković^{*1} Matko Bošnjak^{*1} Thomas Kipf² Alexander Lerchner¹ Raia Hadsell¹ Razvan Pascanu¹
Charles Blundell¹

Abstract

Neural networks leverage robust internal representations in order to generalise. Learning them is difficult, and often requires a large training set that covers the data distribution densely. We study a common setting where our task is not purely opaque. Indeed, very often we may have access to information about the underlying system (e.g. that observations must obey certain laws of physics) that any “tabula rasa” neural network would need to re-learn from scratch, penalising data efficiency. We incorporate this information into a pre-trained reasoning module, and investigate its role in shaping the discovered representations in diverse self-supervised learning settings from pixels. Our approach paves the way for a new class of data-efficient representation learning.

1. Introduction

Neural networks are able to learn policies in environments without access to their specifics (Schrittwieser et al., 2020), generate large quantities of text (Brown et al., 2020), or automatically fold proteins to high accuracy (Senior et al., 2020). However, such “tabula rasa” approaches hinge on having access to substantial quantities of data, from which robust representations can be learned. Without a large training set that spans the data distribution, representation learning is difficult (Belkin et al., 2019; LeCun, 2018; Sun et al., 2017).

In this work, we study ways to construct neural networks with representations that are robust, while retaining a data-driven approach. We rely on a simple observation: very often, we have some (partial) knowledge of the underlying dynamics of the data, which could help make stronger predictions from fewer observations. This knowledge, however, usually requires us to be mindful of *abstract* properties of the data—and such properties cannot always be robustly

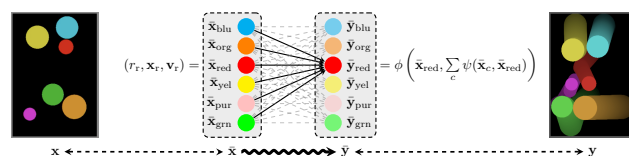


Figure 1. Bouncing balls example (re-printed, with permission, from (Battaglia et al., 2016)). Natural inputs, \mathbf{x} , correspond to pixel observations. Predicting future observations (natural outputs, \mathbf{y}), can be simplified as follows: if we are able to extract a set of *abstract* inputs, $\bar{\mathbf{x}}$, (e.g. the radius, position and velocity for each ball), the movements in this space must obey the laws of physics.

extracted from *natural* observations.

Motivation Consider the task of predicting the future state of a system of n bouncing balls, from a pixel input \mathbf{x} (Figure 1). Reliably estimating future pixel observations, \mathbf{y} , is a challenging reconstruction task. However, the generative properties of this system are simple. Assuming knowledge of simple abstract inputs (radius, r_c , position, \mathbf{x}_c , and velocity, \mathbf{v}_c) for every ball, $\bar{\mathbf{x}}_c$, the future movements in this abstract space are the result of applying the laws of physics to these low-dimensional quantities. Hence, future abstract states, $\bar{\mathbf{y}}$, can be computed via a simple algorithm that aggregates pair-wise forces between objects.

While this gives us a potentially simpler path from pixel inputs to pixel outputs, via abstract inputs to abstract outputs ($\mathbf{x} \rightarrow \bar{\mathbf{x}} \rightsquigarrow \bar{\mathbf{y}} \rightarrow \mathbf{y}$), it still places potentially unrealistic demands on our task setup, every step of the way:

- $\mathbf{x} \rightarrow \bar{\mathbf{x}}$: Necessitates either upfront knowledge of how to abstract away $\bar{\mathbf{x}}$ from \mathbf{x} , or a massive dataset of *paired* $(\mathbf{x}, \bar{\mathbf{x}})$ to learn such a mapping from;
- $\bar{\mathbf{x}} \rightsquigarrow \bar{\mathbf{y}}$: Implies that the algorithm *perfectly* simulates all aspects of the output. In reality, an algorithm may often only give partial context about \mathbf{y} . Further, algorithms often assume that \mathbf{x} is provided without error, exposing an algorithmic bottleneck (Deac et al., 2020): if $\bar{\mathbf{x}}$ is incorrectly predicted, this will negatively compound in $\bar{\mathbf{y}}$, hence \mathbf{y} ;
- $\bar{\mathbf{y}} \rightarrow \mathbf{y}$: Necessitates a renderer that generates \mathbf{y} from $\bar{\mathbf{y}}$, or a dataset of *paired* $(\bar{\mathbf{y}}, \mathbf{y})$ to learn such a mapping.

^{*}Equal contribution ¹DeepMind ²Google Research, Brain Team. Correspondence to: Petar Veličković <petarv@deepmind.com>, Matko Bošnjak <matko@deepmind.com>.

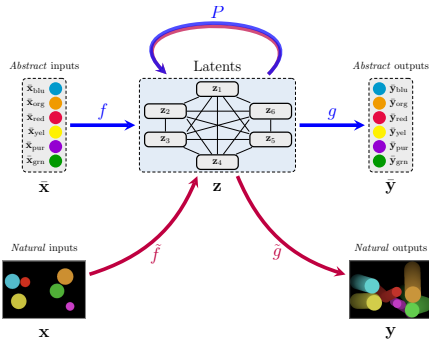


Figure 2. Reasoning-modulated representation learner (RMR).

We will assume a general setting where *none* of the above constraints hold: we know that the mapping $\bar{\mathbf{x}} \rightsquigarrow \bar{\mathbf{y}}$ is likely of use to our predictor, but we do not assume a trivial mapping or a paired dataset which would allow us to convert directly from \mathbf{x} to $\bar{\mathbf{x}}$ or from $\bar{\mathbf{y}}$ to \mathbf{y} . Our only remaining assumption is that the algorithm $\bar{\mathbf{x}} \rightsquigarrow \bar{\mathbf{y}}$ can be efficiently computed, allowing us to generate massive quantities of paired abstract input-output pairs, $(\bar{\mathbf{x}}, \bar{\mathbf{y}})$.

Present work In this setting, we propose Reasoning-Modulated Representations (RMR), an approach that first learns a latent-space *processor* of abstract data; i.e. a mapping $\bar{\mathbf{x}} \xrightarrow{f} \mathbf{z} \xrightarrow{P} \mathbf{z}' \xrightarrow{g} \bar{\mathbf{y}}$, where $\mathbf{z} \in \mathbb{R}^k$ are high-dimensional latent vectors. f and g are an encoder and decoder, designed to take abstract representations to and from this latent space, and P is a processor network which simulates the algorithm $\bar{\mathbf{x}} \rightsquigarrow \bar{\mathbf{y}}$ in the latent space.

We then observe, in the spirit of neural algorithmic reasoning (Veličković & Blundell, 2021), that such a processor network can be used as a drop-in differentiable component for *any* task where the $\bar{\mathbf{x}} \rightsquigarrow \bar{\mathbf{y}}$ kind of reasoning may be applicable. Hence, we then learn a pipeline $\mathbf{x} \xrightarrow{\hat{f}} \mathbf{z} \xrightarrow{P} \mathbf{z}' \xrightarrow{\hat{g}} \mathbf{y}$, which *modulates* the representations \mathbf{z} obtained from \mathbf{x} , forcing them to pass through the pre-trained processor network. By doing so, we have ameliorated the original requirement for a massive *natural* dataset of (\mathbf{x}, \mathbf{y}) pairs. Instead, we inject knowledge from a massive *abstract* dataset of $(\bar{\mathbf{x}}, \bar{\mathbf{y}})$ pairs, directly through the pre-trained parameters of P . This has the potential to relieve the pressure on encoders and decoders f and g , which we experimentally validate on several challenging representation learning domains.

2. RMR architecture

Throughout this section, it will be useful to refer to Figure 2 which presents a visual overview of this section.

Preliminaries We assume a set of *natural inputs*, \mathcal{X} , and a set of *natural outputs*, \mathcal{Y} . These sets represent the possible

inputs and outputs of a target function, $\Phi : \mathcal{X} \rightarrow \mathcal{Y}$, which we would like to learn based on a (potentially small) dataset of input-output pairs, (\mathbf{x}, \mathbf{y}) , where $\mathbf{y} = \Phi(\mathbf{x})$.

We further assume that the inner workings of Φ can be related to an *algorithm*, $A : \bar{\mathcal{X}} \rightarrow \bar{\mathcal{Y}}$. The algorithm operates over a set of *abstract inputs*, $\bar{\mathcal{X}}$, and produces outputs from an *abstract output set* $\bar{\mathcal{Y}}$. Typically, it will be the case that $\dim \bar{\mathcal{X}} \ll \dim \mathcal{X}$; that is, abstract inputs are assumed substantially lower-dimensional than natural inputs. We do not assume existence of any aligned input pairs $(\mathbf{x}, \bar{\mathbf{x}})$, and we do not assume that A perfectly explains the computations of Φ . What we do assume is that A is either known or can be trivially computed, giving rise to a massive dataset of abstract input-output pairs, $(\bar{\mathbf{x}}, \bar{\mathbf{y}})$, where $\bar{\mathbf{y}} = A(\bar{\mathbf{x}})$.

Lastly, we assume a *latent space*, \mathcal{Z} , and that we can construct neural network components to both encode and decode from it. Typically, \mathcal{Z} will be a real-valued vector space ($\mathcal{Z} = \mathbb{R}^k$) which is high-dimensional; that is, $k > \dim \bar{\mathcal{X}}$. This ensures that any neural networks operating over \mathcal{Z} are not vulnerable to bottleneck effects.

Note that either the natural or abstract input set may be *factorised*, e.g., into objects; in this case, we can accordingly factorise the latent space, enforcing $\mathcal{Z} = \mathbb{R}^{n \times k}$, where n is the assumed maximal number of objects (typically a hyperparameter of the models if not known upfront).

Abstract pipeline RMR training proceeds by first learning a model of the algorithm A , which is bound to pass through a latent-space representation. That is, we learn a neural network approximator $g(P(f(\bar{\mathbf{x}}))) \approx A(\bar{\mathbf{x}})$, which follows the encode-process-decode paradigm (Hamrick et al., 2018). It consists of the following three building blocks: Encoder, $f : \bar{\mathcal{X}} \rightarrow \mathcal{Z}$, tasked with projecting the abstract inputs into the latent space; Processor, $P : \mathcal{Z} \rightarrow \mathcal{Z}$, simulating individual steps of the algorithm in the latent space; Decoder, $g : \mathcal{Z} \rightarrow \bar{\mathcal{Y}}$, tasked with projecting latents back into the abstract output space.

Natural pipeline Once an appropriate processor, P , has been learned, it may be observed that it corresponds to a highly favourable component in our setting. Namely, we can relate its operations to the algorithm A , and since it stays high-dimensional, it is a differentiable component we can easily plug into other neural networks without incurring any bottleneck effects. This insight was originally recovered in XLVIN (Deac et al., 2020), where it yielded a generic implicit planner. We now leverage similar insights for general representation learning tasks.

On a high level, what we need to do is simple and elegant: swap out f and g for *natural* encoders and decoders, $\hat{f} : \mathcal{X} \rightarrow \mathcal{Z}$ and $\hat{g} : \mathcal{Z} \rightarrow \mathcal{Y}$, respectively. We are then able to learn a function $\hat{g}(P(\hat{f}(\mathbf{x}))) \approx \Phi(\mathbf{x})$, which is once again

to be optimised through gradient descent. We would like P to retain its semantics during training, and therefore it is typically kept *frozen* in the natural pipeline.

3. RMR for bouncing balls

To evaluate the capability of the RMR pipeline for transfer from the abstract space to the pixel space, we apply it on the “bouncing balls” problem. The bouncing balls problem is an instance of a physics simulation problem, where the task is to predict the next state of an environment in which multiple balls are bouncing between each other and a bounding box. Though this problem had been studied in the the context of physics simulation from (abstract) trajectories (Battaglia et al., 2016) and from (natural) videos (Watters et al., 2017; Van Steenkiste et al., 2018; Löwe et al., 2020), here we focus on the aptitude of RMR to transfer learned representations from trajectories to videos.

Our results affirm that strong abstract models can be trained on such tasks, and that including them in a video pipeline induces more robust representations. See Appendix A for more details on hyperparameters and experimental setup.

Preliminaries In this setting, trajectories are represented by 2D coordinates of 10 balls through time, defining our abstract inputs and outputs $\bar{\mathcal{X}} = \bar{\mathcal{Y}} = \mathbb{R}^{10 \times 2}$. We slice these trajectories into a series of moving windows containing the input, $\bar{\mathbf{x}}^*$, spanning a history of three previous states, and the target, $\bar{\mathbf{y}}$, representing the next state. We obtain these trajectories from a 3D simulator (MuJoCo (Todorov et al., 2012)), together with their short-video renderings, which represent our natural input and output space $\mathcal{X} = \mathcal{Y} = \mathbb{R}^{64 \times 64 \times 3}$. Our goal is to train an RMR abstract model on trajectories and transfer learned representations to improve a dynamics model trained on these videos.

Abstract pipeline So as to model the dynamics of trajectories, we closely follow the RMR desiderata for the abstract model. We set f to a linear projection over the input concatenation, P to a Message Passing Neural Network (MPNN), following previous work (Battaglia et al., 2016; Sanchez-Gonzalez et al., 2020), and g to a linear projection.

Our model learns a transition function $g(P(f(\bar{\mathbf{x}}^*)) \approx \bar{\mathbf{y}}$, supervised using Mean Squared Error (MSE) over ball positions in the next step. It achieves an MSE of 4.59×10^{-4} , which, evaluated qualitatively, demonstrates the ability of the model to predict physically realistic behavior when unrolled for 10 steps (the model is trained on 1-step dynamics only). Next, we take the processor P from the abstract pipeline and re-use it in the natural pipeline.

Natural pipeline Here we evaluate whether the pre-trained RMR processor can be reused for learning the dy-



Figure 3. RMR for bouncing balls reconstruction rollout. States marked in green are the natural input, followed by the reconstructed output. The states below the reconstruction is the ground truth.

namics of the bouncing balls from videos. The pixel-based encoder \bar{f} is concatenation of per-input-image Slot Attention model (Locatello et al., 2020), passed through a linear layer, and a Broadcast Decoder (Watters et al., 2019) for the pixel-based decoder \bar{g} .

The full model is a transition function $\bar{g}(P(\bar{f}(\mathbf{x}^*)) \approx \mathbf{y}$, supervised by pixel reconstruction loss over the next step image. We compare the performance of the RMR model with a pre-trained processor P against a baseline in which P is trained fully end-to-end. The RMR model achieves an MSE of $7.94 \pm 0.41 (\times 10^{-4})$, whereas the baseline achieves $9.47 \pm 0.24 (\times 10^{-4})$. We take a qualitative look at the reconstruction rollout of the RMR model in Figure 3.

4. Contrastive RMR for Atari

We evaluate the potential of our RMR pipeline for data-efficient state representation learning on the Atari 2600 console (Bellemare et al., 2013). We find that the RMR is applicable in this setting because there is a potential wealth of information that can be obtained about the Atari’s mode of operation—namely, by inspecting its RAM traces.

Preliminaries Accordingly, we will define our set of abstract inputs and outputs as Atari RAM matrices. Given that the Atari has 128 bytes of memory, $\bar{\mathcal{X}} = \bar{\mathcal{Y}} = \mathbb{B}^{128 \times 8}$ (where $\mathbb{B} = \{0, 1\}$ is the set of bits). We collect data about how the console modifies the RAM by acting in the environment and recording the trace of RAM arrays we observe. These traces will be of the form $(\bar{\mathbf{x}}, a, \bar{\mathbf{y}})$ which signify that the agent’s initial RAM state was $\bar{\mathbf{x}}$, and that after performing action $a \in \mathcal{A}$, its RAM state was updated to $\bar{\mathbf{y}}$. We assume that a is encoded as an 18-way one-hot vector.

We would like to leverage any reasoning module obtained over RAM states to support representation learning from raw pixels. Accordingly, our natural inputs, \mathcal{X} , are pixel arrays representing the Atari’s framebuffer.

Mirroring prior work, we perform contrastive learning directly in the latent space, and set $\mathcal{Y} = \mathcal{Z}$; that is, our natural outputs correspond to an estimate of the “updated” latents after taking an action. All our models use latent representations of 64 dimensions per slot, meaning $\mathcal{Z} = \mathbb{R}^{128 \times 64}$.

We note that it is important to generate a diverse dataset of experiences in order to train a robust RAM model. To simulate as closely as possible a dataset which might be gathered by human players of varying skill level, we sample our data using the 32 policy heads of a pre-trained Agent57 model (Badia et al., 2020). Each policy head collects data over three episodes in the studied games. Note that this implies a substantially more challenging dataset than the one reported by (Anand et al., 2019), wherein data was collected by a purely random policy, which may well fail to explore many relevant regions of the games.

Abstract pipeline Firstly, we set out to verify that it is possible to train nontrivial Atari RAM transition models. The construction of this abstract experiment follows almost exactly the abstract RMR setup: f and g are appropriately sized linear projections, while P needs to take into account which action was taken when updating the latents. To simplify the implementation and allow further model re-use, we consider the action a part of the P ’s inputs.

This implies that our transition model learns a function $g(P(f(\bar{x}), a)) \approx \bar{y}$. We supervise this model using binary cross-entropy to predict each bit of the resulting RAM state. Since RAM transitions are assumed deterministic, we assume a fully Markovian setup and learn 1-step dynamics.

For brevity purposes, we detail our exact hyperparameters and results per each Atari game considered in Appendix B. Our results ascertain the message passing neural network (MPNN) (Gilmer et al., 2017) as a highly potent processor network in Atari: it ranked most potent in 14 out of 19 games considered, compared to MLPs and Deep Sets (Zaheer et al., 2017). Accordingly, we will focus on leveraging pre-trained MPNN processors for the next phase of the RMR pipeline.

Natural pipeline We now set out to evaluate whether our pre-trained RMR processors can be meaningfully re-used by an encoder in a pixel-based contrastive learning pipeline.

For our pixel-based encoder \tilde{f} , we use the same CNN trunk as in (Anand et al., 2019)—however, as we require slot-level rather than image-level embeddings, the final layers of our encoder are different. Namely, we apply a 1×1 convolution computing $128m$ feature maps (where m is the number of feature maps per-slot). We then flatten the spatial axes, giving every slot $m \times h \times w$ features, which we finally linearly project to 64-dimensional features per-slot, aligning with our pre-trained P . Note that setting $m = 1$ recovers exactly the style of object detection employed by C-SWM (Kipf et al., 2019). Since our desired outputs are themselves latents, \tilde{g} is a single linear projection to 64 dimensions.

Overall, our pixel-based transition model learns a function $\tilde{g}(P(\tilde{f}(\mathbf{x}), a)) \approx \tilde{f}(\mathbf{y})$, where \mathbf{y} is the next state observed after applying action a in state \mathbf{x} . To optimise it, we re-

Table 1. Natural modelling results for Atari 2600. Bit-level F₁ reported for slots with high entropy, as in (Anand et al., 2019). Results are considered **significant** at $p < 0.05$ (paired t -test).

Game	C-SWM	RMR	p -value
Asteroids	0.597±0.002	0.602 ±0.003	0.006
Berzerk	0.533±0.022	0.528±0.033	0.368
Bowling	0.949±0.003	0.951±0.002	0.110
Boxing	0.667±0.011	0.678 ±0.006	0.040
Breakout	0.839±0.014	0.868 ±0.003	0.002
Freeway	0.917±0.018	0.938 ±0.003	0.020
Frostbite	0.596±0.020	0.641 ±0.008	0.004
H.E.R.O.	0.799±0.016	0.845 ±0.016	0.004
Montezuma	0.829±0.006	0.829±0.023	0.490
Ms. Pac-Man	0.606±0.005	0.604±0.003	0.246
Pitfall!	0.608±0.008	0.633 ±0.016	0.012
Pong	0.765±0.009	0.774 ±0.004	0.025
Private Eye	0.859±0.009	0.874 ±0.007	0.043
River Raid	0.764±0.003	0.771 ±0.002	0.008
Skiing	0.770±0.009	0.769±0.017	0.345
Space Invaders	0.779±0.004	0.779±0.003	0.363
Tennis	0.728±0.003	0.735 ±0.002	0.004
Venture	0.637±0.005	0.639±0.002	0.337
Yars’ Revenge	0.772±0.002	0.778 ±0.001	0.002

use exactly the same TransE-inspired (Bordes et al., 2013) contrastive loss that C-SWM (Kipf et al., 2019) used.

Once state representation learning concludes, all components are typically thrown away except for the encoder, \tilde{f} , which is used for downstream tasks. As a proxy for evaluating the quality of the encoder, we train linear classifiers on the concatenation of all slot embeddings obtained from \tilde{f} to predict individual RAM bits, exactly as in the abstract model case. Note that, by doing this, we have *not* violated our assumption that paired $(\mathbf{x}, \bar{\mathbf{x}})$ samples will not be provided while training the natural model—in this phase of RAM probing, the encoder \tilde{f} is frozen, and gradients can only flow into the linear probe.

Our comparisons for this experiment, evaluating our RMR pipeline against an identical architecture with an unfrozen P (equivalent to C-SWM (Kipf et al., 2019)) is provided in Table 1. For each of five random seeds, we feed identical batches to both models, hence we can perform a paired t -test to assess the statistical significance of any observed differences on validation episodes. The results are in line with our expectations: representations learnt by RMR are significantly better ($p < 0.05$) on 12 out of 19 games—and indistinguishable to C-SWM’s on others. This is despite the fact their architectures are identical, indicating that the pre-trained abstract model induces stronger representations for predicting the underlying factors of the data.

Acknowledgements

We would like to thank the developers of JAX (Bradbury et al., 2018) and Haiku (Hennigan et al., 2020). Further, we are very thankful to Adrià Puigdomènech Badia, Steven Kapturowski, Ankesh Anand, Richard Evans, Yulia Rubanova, Alvaro Sanchez-Gonzalez and Bojan Vujatović for their invaluable advice prior to submission.

TK is a Research Scientist at Google Research, Brain Team. All other authors are Research Scientists at DeepMind.

References

- Anand, A., Racah, E., Ozair, S., Bengio, Y., Côté, M.-A., and Hjelm, R. D. Unsupervised state representation learning in atari. *arXiv preprint arXiv:1906.08226*, 2019.
- Badia, A. P., Piot, B., Kapturowski, S., Sprechmann, P., Vitvitskiy, A., Guo, Z. D., and Blundell, C. Agent57: Outperforming the atari human benchmark. In *International Conference on Machine Learning*, pp. 507–517. PMLR, 2020.
- Battaglia, P. W., Pascanu, R., Lai, M., Rezende, D., and Kavukcuoglu, K. Interaction networks for learning about objects, relations and physics. *arXiv preprint arXiv:1612.00222*, 2016.
- Belkin, M., Hsu, D., Ma, S., and Mandal, S. Reconciling modern machine-learning practice and the classical bias-variance trade-off. *Proceedings of the National Academy of Sciences*, 116(32):15849–15854, 2019.
- Bellemare, M. G., Naddaf, Y., Veness, J., and Bowling, M. The arcade learning environment: An evaluation platform for general agents. *Journal of Artificial Intelligence Research*, 47:253–279, 2013.
- Bordes, A., Usunier, N., Garcia-Duran, A., Weston, J., and Yakhnenko, O. Translating embeddings for modeling multi-relational data. In *Neural Information Processing Systems (NIPS)*, pp. 1–9, 2013.
- Bradbury, J., Frostig, R., Hawkins, P., Johnson, M. J., Leary, C., Maclaurin, D., and Wanderman-Milne, S. JAX: composable transformations of Python+NumPy programs, 2018. URL <http://github.com/google/jax>.
- Brown, T. B., Mann, B., Ryder, N., Subbiah, M., Kaplan, J., Dhariwal, P., Neelakantan, A., Shyam, P., Sastry, G., Askell, A., et al. Language models are few-shot learners. *arXiv preprint arXiv:2005.14165*, 2020.
- Deac, A., Veličković, P., Milinković, O., Bacon, P.-L., Tang, J., and Nikolić, M. Xlvin: executed latent value iteration nets. *arXiv preprint arXiv:2010.13146*, 2020.
- Gilmer, J., Schoenholz, S. S., Riley, P. F., Vinyals, O., and Dahl, G. E. Neural message passing for quantum chemistry. In *International Conference on Machine Learning*, pp. 1263–1272. PMLR, 2017.
- Hamrick, J. B., Allen, K. R., Bapst, V., Zhu, T., McKee, K. R., Tenenbaum, J. B., and Battaglia, P. W. Relational inductive bias for physical construction in humans and machines. *arXiv preprint arXiv:1806.01203*, 2018.
- Hennigan, T., Cai, T., Norman, T., and Babuschkin, I. Haiku: Sonnet for JAX, 2020. URL <http://github.com/deepmind/dm-haiku>.
- Kingma, D. P. and Ba, J. Adam: A method for stochastic optimization. *arXiv preprint arXiv:1412.6980*, 2014.
- Kipf, T., van der Pol, E., and Welling, M. Contrastive learning of structured world models. *arXiv preprint arXiv:1911.12247*, 2019.
- LeCun, Y. The power and limits of deep learning. *Research-Technology Management*, 61(6):22–27, 2018.
- Locatello, F., Weissenborn, D., Unterthiner, T., Mahendran, A., Heigold, G., Uszkoreit, J., Dosovitskiy, A., and Kipf, T. Object-centric learning with slot attention. *arXiv preprint arXiv:2006.15055*, 2020.
- Löwe, S., Greff, K., Jonschkowski, R., Dosovitskiy, A., and Kipf, T. Learning object-centric video models by contrasting sets. *arXiv preprint arXiv:2011.10287*, 2020.
- Sanchez-Gonzalez, A., Godwin, J., Pfaff, T., Ying, R., Leskovec, J., and Battaglia, P. Learning to simulate complex physics with graph networks. In *International Conference on Machine Learning*, pp. 8459–8468. PMLR, 2020.
- Santoro, A., Raposo, D., Barrett, D. G., Malinowski, M., Pascanu, R., Battaglia, P., and Lillicrap, T. A simple neural network module for relational reasoning. *arXiv preprint arXiv:1706.01427*, 2017.
- Schrittwieser, J., Antonoglou, I., Hubert, T., Simonyan, K., Sifre, L., Schmitt, S., Guez, A., Lockhart, E., Hassabis, D., Graepel, T., et al. Mastering atari, go, chess and shogi by planning with a learned model. *Nature*, 588(7839): 604–609, 2020.
- Senior, A. W., Evans, R., Jumper, J., Kirkpatrick, J., Sifre, L., Green, T., Qin, C., Žídek, A., Nelson, A. W., Bridgland, A., et al. Improved protein structure prediction using potentials from deep learning. *Nature*, 577(7792): 706–710, 2020.
- Strathmann, H., Barekatin, M., Blundell, C., and Veličković, P. Persistent message passing. *arXiv preprint arXiv:2103.01043*, 2021.

Sun, C., Shrivastava, A., Singh, S., and Gupta, A. Revisiting unreasonable effectiveness of data in deep learning era. In *Proceedings of the IEEE International Conference on Computer Vision (ICCV)*, Oct 2017.

Todorov, E., Erez, T., and Tassa, Y. Mujoco: A physics engine for model-based control. In *2012 IEEE/RSJ International Conference on Intelligent Robots and Systems*, pp. 5026–5033. IEEE, 2012.

Van Steenkiste, S., Chang, M., Greff, K., and Schmidhuber, J. Relational neural expectation maximization: Unsupervised discovery of objects and their interactions. *arXiv preprint arXiv:1802.10353*, 2018.

Veličković, P. and Blundell, C. Neural algorithmic reasoning. *arXiv preprint arXiv:2105.02761*, 2021.

Veličković, P., Buesing, L., Overlan, M. C., Pascanu, R., Vinyals, O., and Blundell, C. Pointer graph networks. *arXiv preprint arXiv:2006.06380*, 2020.

Watters, N., Zoran, D., Weber, T., Battaglia, P., Pascanu, R., and Tacchetti, A. Visual interaction networks: Learning a physics simulator from video. *Advances in neural information processing systems*, 30:4539–4547, 2017.

Watters, N., Matthey, L., Burgess, C. P., and Lerchner, A. Spatial broadcast decoder: A simple architecture for learning disentangled representations in vaes. *arXiv preprint arXiv:1901.07017*, 2019.

Zaheer, M., Kottur, S., Ravanbakhsh, S., Póczos, B., Salakhutdinov, R., and Smola, A. Deep sets. *arXiv preprint arXiv:1703.06114*, 2017.

A. Bouncing balls modelling setup

Abstract pipeline The f is a linear projection over the concatenation of inputs, outputting a 128-long representation for each of the 10 balls in the input. The P is a MPNN over the fully connected graph of the ball representations. It is a 2-pass MPNN with a 3-layered ReLU-activated MLP as a message function, without the final layer activation, projecting to the same 128-dimensional space, per object. Finally, g is a linear projection applied on each object representation of the output of P .

The model is MSE-supervised with ball position on the next step. It is trained on a 8-core TPU for 10000 epochs, with a batch size of 512, and the Adam optimizer with the initial learning rate of 0.0001.

Natural pipeline \bar{f} is a Slot Attention model (Locatello et al., 2020) on each input image, concatenating the images and passing them through a linear layer, outputting a 128-dimensional vector for each of the objects. \bar{g} is a Broadcast

Decoder (Watters et al., 2019) containing a sequence of 5 transposed convolutions and a linear layer mapping before calculating the reconstructions and their masks.

The model is MSE-supervised by pixel reconstruction (per-pixel MSE) over the next step image. Both the RMR and the baseline are trained on a 8-core TPU for 1000 epochs, with a batch size of 512, with the Adam optimiser and the initial learning rate of 0.0001, all over 3 random seeds.

B. Atari abstract modelling setup and results

Our best processor network is a MPNN (Gilmer et al., 2017) over a fully connected graph (Santoro et al., 2017) of RAM slots, which concatenates the action embedding to every node (as done in (Kipf et al., 2019)). It uses three-layer MLPs as message functions, with the ReLU activation applied after each hidden layer. The entire model is trained for every game in isolation, over 48 distinct episodes of Agent57 experience. We use the Adam SGD optimiser (Kingma & Ba, 2014) with a batch size of 50 and a learning rate of 0.001 across all Atari experiments. To evaluate the benefits of message passing, we also compare our model to Deep Sets (Zaheer et al., 2017), which is equivalent to our MPNN model—only it passes messages over the identity adjacency matrix. Lastly, we evaluate the benefits of factorised latents by comparing our methods against a three-layer MLP applied on the flattened RAM state.

One immediate observation is that RAM updates in Atari are extremely sparse, with a *copy baseline* already being very strong for many games. To prevent the model from having to repeatedly re-learn identity functions, we also make it predict *masks* of the shape $\mathcal{M} = \mathbb{B}^{128}$, specifying which cells are to be overwritten by the model at this step. This strategy, coupled with teacher forcing (as done by (Veličković et al., 2020; Strathmann et al., 2021)) yielded substantially stronger predictors. We also use this observation to prevent over-inflating our prediction scores: we only display prediction accuracy over RAM slots with label entropy larger than 0.6 (as done by (Anand et al., 2019)).

The full results of training Atari RAM transition models, for the games studied in (Anand et al., 2019), are provided in Table 2. We evaluate both bit-level F_1 scores, as well as slot-level accuracy (for which all 8 bits need to be predicted correctly in order to count), over the remaining 48 Agent57 episodes as validation. To the best of our knowledge, this is the first comprehensive feasibility study for learning Atari RAM transition models.

Table 2. Abstract modelling results for Atari 2600. Entire-slot accuracies and bit-level F_1 scores are reported only for slots with high entropy, as per (Anand et al., 2019).

Game	Copy baseline		MLP		Deep Sets		MPNN	
	Slot acc.	Bit F_1	Slot acc.	Bit F_1	Slot acc.	Bit F_1	Slot acc.	Bit F_1
Asteroids	70.65%	0.856	71.28%	0.872	72.84%	0.879	80.69%	0.930
Berzerk	84.32%	0.905	86.17%	0.930	84.16%	0.923	86.67%	0.933
Bowling	93.86%	0.972	97.43%	0.991	90.72%	0.966	98.41%	0.995
Boxing	59.78%	0.848	54.45%	0.834	59.79%	0.890	58.56%	0.877
Breakout	89.80%	0.949	92.77%	0.970	94.34%	0.979	96.45%	0.988
Freeway	46.65%	0.787	75.93%	0.921	84.68%	0.959	89.17%	0.965
Frostbite	76.83%	0.904	79.09%	0.904	78.25%	0.946	76.52%	0.918
H.E.R.O.	76.71%	0.891	82.96%	0.932	80.17%	0.929	89.07%	0.956
Montezuma’s Revenge	82.58%	0.907	87.30%	0.941	85.90%	0.951	85.44%	0.932
Ms. Pac-Man	83.80%	0.941	80.60%	0.935	81.50%	0.952	85.88%	0.966
Pitfall!	66.60%	0.862	78.28%	0.923	81.92%	0.947	80.40%	0.941
Pong	68.76%	0.873	73.58%	0.911	74.71%	0.920	83.23%	0.952
Private Eye	75.25%	0.889	81.95%	0.932	84.77%	0.954	86.41%	0.955
River Raid	76.95%	0.895	80.82%	0.927	69.96%	0.865	86.79%	0.954
Skiing	91.02%	0.966	93.42%	0.980	93.51%	0.983	96.37%	0.992
Space Invaders	81.67%	0.942	84.62%	0.957	89.38%	0.974	91.98%	0.985
Tennis	78.13%	0.890	82.13%	0.926	71.60%	0.856	80.20%	0.893
Venture	61.29%	0.858	63.16%	0.863	64.88%	0.886	76.56%	0.935
Yars’ Revenge	69.25%	0.896	74.87%	0.929	72.69%	0.948	84.11%	0.969